Early life of Neanderthals

Alessia Nava[a,b,1,2], Federico Lugli[c,d,1,2], Matteo Romandini[c,e], Federica Badino[c,f], David Evans[g,h], Angela H. Helbling[g,h], Gregorio Oxilia[c], Simona Arrighi[c], Eugenio Bortolini[c], Davide Delpiano[i], Rossella Duches[j], Carla Figus[c], Alessandra Livraghi[i,k], Giulia Marciani[c], Sara Silvestrini[c], Anna Cipriani[d,l], Tommaso Giovanardi[d], Roberta Pini[f], Claudio Tuniz[m,n,o], Federico Bernardini[m,n], Irene Dori[p,q], Alfredo Coppa[r,s,t], Emanuela Cristiani[a], Christopher Dean[u,v], Luca Bondioli[w,x], Marco Peresani[f,i,2], Wolfgang Müller[g,h,2], and Stefano Benazzi[c,y,2]

[a]DANTE–Diet and Ancient Technology Laboratory, Department of Maxillo-Facial Sciences, Sapienza University of Rome, 00161 Rome, Italy; [b]Skeletal Biology Research Centre, School of Anthropology and Conservation, University of Kent, Canterbury CT2 7NZ, United Kingdom; [c]Department of Cultural Heritage, University of Bologna, 48121 Ravenna, Italy; [d]Department of Chemical and Geological Sciences, University of Modena and Reggio Emilia, 41125 Modena, Italy; [e]Pradis Cave Museum, 33090 Clauzetto, Italy; [f]Institute of Environmental Geology and Geoengineering–IGAG CNR, 20131 Milan, Italy; [g]Institute of Geosciences, Goethe University Frankfurt, 60438 Frankfurt am Main, Germany; [h]Frankfurt Isotope and Element Research Center (FIERCE), Goethe University Frankfurt, 60438 Frankfurt am Main, Germany; [i]Department of Humanities, 44121 Ferrara, University of Ferrara, Italy; [j]Prehistory Section–MuSe, Museum of Science, 38122 Trento, Italy; [k]Area de Prehistoria, University Rovira i Virgili, 43002 Tarragona, Spain; [l]Lamont-Doherty Earth Observatory of Columbia University, Palisades, NY 10964-1000; [m]Multidisciplinary Laboratory, Abdus Salam International Centre for Theoretical Physics, 34151 Trieste, Italy; [n]Centro Fermi, Museo Storico della Fisica e Centro di Studi e Ricerche Enrico Fermi, 00184 Roma, Italy; [o]Center for Archaeological Science, University of Wollongong, Wollongong, NSW 2522, Australia; [p]Soprintendenza Archeologia, Belle Arti e Paesaggio per le province di Verona, Rovigo e Vicenza, 37121 Verona, Italy; [q]Department of Biology, Laboratory of Anthropology, University of Florence, 50122 Florence, Italy; [r]Department of Environmental Biology, Sapienza University of Rome, 00185 Rome, Italy; [s]Department of Genetics, Harvard Medical School, Boston, MA 02115; [t]Department of Evolutionary Anthropology, University of Vienna, 1090 Vienna, Austria; [u]Department of Earth Sciences, Natural History Museum, London SW7 5BD, United Kingdom; [v]Department of Cell and Developmental Biology, University College London, London WC1E 6BT, United Kingdom; [w]Bioarchaeology Service, Museum of Civilization, 00144 Rome, Italy; [x]Department of Cultural Heritage, University of Padua, 35139 Padua, Italy; and [y]Department of Human Evolution, Max Planck Institute for Evolutionary Anthropology, 04103 Leipzig, Germany

Edited by Noreen Tuross, Harvard University, Cambridge, MA, and accepted by Editorial Board Member Richard G. Klein September 21, 2020 (received for review June 8, 2020)

The early onset of weaning in modern humans has been linked to the high nutritional demand of brain development that is intimately connected with infant physiology and growth rate. In Neanderthals, ontogenetic patterns in early life are still debated, with some studies suggesting an accelerated development and others indicating only subtle differences vs. modern humans. Here we report the onset of weaning and rates of enamel growth using an unprecedented sample set of three late (~70 to 50 ka) Neanderthals and one Upper Paleolithic modern human from northeastern Italy via spatially resolved chemical/isotopic analyses and histomorphometry of deciduous teeth. Our results reveal that the modern human nursing strategy, with onset of weaning at 5 to 6 mo, was present among these Neanderthals. This evidence, combined with dental development akin to modern humans, highlights their similar metabolic constraints during early life and excludes late weaning as a factor contributing to Neanderthals' demise.

Neanderthal ontogeny | nursing strategy | dental histology | spatially resolved chemical analyses | life histories

Maternal physiology, breastfeeding, and the first introduction of supplementary foods are key determinants of human growth (1). The high nutritional demands of the human brain during the first years of life has been identified as the main reason for the early weaning onset in modern humans (2, 3). Indeed, supplementary food is needed when an infant's nutritional requirements exceed what the mother can provide through breastmilk only (4), and this dietary development can introduce foods that are higher in protein, calories, and key micronutrients than maternal milk (4, 5). Weaning onset occurs in contemporary nonindustrial human societies at a modal age of 6 mo (6).

At present, our knowledge about the link between the pace of child growth, maternal behavior, and the onset of weaning among Neanderthals is still limited. Previous work based on permanent teeth from eight Neanderthal specimens reported that Neanderthal tooth crowns tend to develop faster than in modern humans, suggesting infant growth was generally accelerated (7). However, a permanent first molar and a second deciduous molar from La Chaise (France; 127 to 116 ka and <163 ka, respectively) placed rates of Neanderthal tooth growth within the range of modern humans (8). Equally, the association between dental and skeletal growth in a 7-y-old Neanderthal from El Sidrón (Spain; 49 ka) indicated that Neanderthals and modern humans were similar in terms of ontogenetic development, with only small-scale dissimilarities in acceleration or deceleration of skeletal maturation (9). Finally, other work suggested that the early growth of the Neanderthal brain was as fast as in modern humans with similar energetic demands (10). Maps of Ba/Ca ratios of permanent tooth

Significance

The extent to which Neanderthals differ from us is the focus of many studies in human evolution. There is debate about their pace of growth and early-life metabolic constraints, both of which are still poorly understood. Here we use chemical and isotopic patterns in tandem with enamel growth rates of three Neanderthal milk teeth from northeastern Italy to explore the early life of these individuals. Our study shows that these Neanderthals started to wean children at 5 to 6 months, akin to modern humans, implying similar energy demands during early infancy. Dental growth rates confirm this and follow trajectories comparable with modern humans. Contrary to previous evidence, we suggest that differences in weaning age did not contribute to Neanderthals' demise.

Author contributions: A.N., F.L., M.R., C.D., L.B., M.P., W.M., and S.B. designed research; A.N., F.L., D.E., A.H.H., S.S., A. Cipriani, T.G., C.D., L.B., W.M., and S.B. performed research; S.A., D.D., R.D., C.F., A.L., G.M., R.P., C.T., F. Bernardini, I.D., A. Coppa, and E.C. contributed new reagents/analytic tools; A.N., F.L., D.E., A.H.H., G.O., E.B., L.B., W.M., and S.B. analyzed data; A.N., F.L., M.R., F. Badino, D.E., C.D., L.B., M.P., W.M., and S.B. wrote the paper; M.R., D.D., R.D., A.L., and M.P. coordinated archaeological excavations; F. Badino and R.P. produced ecological framework; A.H.H. and A. Cipriani revised the manuscript; G.O., S.A., C.F., G.M., I.D., A. Coppa, and E.C. curated, sampled and/or described analyzed teeth; and C.T. and F. Bernardini produced the microtomographic record.

The authors declare no competing interest.

This article is a PNAS Direct Submission. N.T. is a guest editor invited by the Editorial Board.

[1]A.N. and F.L. contributed equally to this work.

[2]To whom correspondence may be addressed. Email: alessia.nava@uniroma1.it, federico.lugli6@unibo.it, marco.peresani@unife.it, w.muller@em.uni-frankfurt.de, or stefano.benazzi@unibo.it.

This article contains supporting information online at https://www.pnas.org/lookup/suppl/doi:10.1073/pnas.2011765117/-/DCSupplemental.

First published November 2, 2020.

sections of two early Neanderthals (Payre 6, 250 ka; and Scladina, 120 ka) have been interpreted (controversially; see below) as indicators of weaning onset at ∼9 mo (11) and 7 mo (12) of age, respectively, later than the modal age in contemporary humans (6). Similarly, wear-stage analyses of a large number of deciduous dentitions suggested that introduction of solid food in Neanderthals was delayed by 1 y compared to modern humans (13).

Here we investigate such key aspects of early life in Neanderthals by combining new data on chemical detection of weaning onset with deciduous enamel growth rates. We utilize dental histomorphometry (8, 14) and spatially resolved chemical (15) and isotopic profiles (16, 17) of dental enamel to reconstruct growth rates (14), nursing practices (4), and mobility (16) at high time resolution (up to weekly). We analyzed an unprecedented set of teeth (n = 4; *SI Appendix*, Text S1) from adjacent archaeological sites in northeastern Italy (*SI Appendix*, Text S2), dated from the Late Middle to the Early Upper Paleolithic, from Neanderthal–modern human contexts (70 to 40 ka). These four exfoliated deciduous fossil teeth include three Neanderthals [Nadale 1, a lower right deciduous first molar (18), ∼70 ka; Fumane 1, a lower left deciduous second molar (19), ∼50 ka; Riparo Broion 1, an upper left deciduous canine (20), ∼50 ka] and one Early Upper Paleolithic modern human (UPMH) as a comparative specimen from the Fumane site [Fumane 2, an upper right deciduous second incisor (21), Protoaurignacian, ∼40 ka; Fig. 1 (22, 23)].

Exfoliated deciduous teeth derive from individuals who survived permanent tooth replacement and were thus unaffected by any mortality-related bias (24). All teeth come from the same geographic area within a ∼55-km radius (Fig. 1), and Fumane 1 and 2 were recovered from different archaeological layers in the same cave, thus allowing direct comparisons in a well-constrained ecogeographical setting.

We quantified enamel incremental growth parameters such as postnatal crown formation time and daily enamel secretion rates (25), and we detected the presence of the neonatal line as birth marker (26) by optical light microscopy on thin sections of the deciduous dental crowns. Weaning onset was investigated via Sr/Ca profiles on the same histological sections along the enamel–dentine junction (EDJ) by laser-ablation inductively coupled plasma mass spectrometry (LA-ICPMS) (15). In order to detect mobility and/or potential nonlocal food sources in maternal diet, $^{87}Sr/^{86}Sr$ isotope ratio profiles were measured by LA multicollector ICPMS (*Materials and Methods*) (16, 17). Moreover, we evaluated elemental ratio profiles in teeth from children with known life history (*SI Appendix*, Text S3) (15).

Results

The neonatal lines marking birth were visible in all four archaeological specimens, despite their worn crowns (*SI Appendix*, Fig. S1), allowing the precise estimation of postnatal crown formation times (Fig. 2*A*). The deciduous first molar Nadale 1 and the deciduous canine Riparo Broion 1 lie within the modern human variability (27–30), while the second deciduous molar Fumane 1 shows a shorter postnatal crown formation time compared with the known archaeological and modern human range (27). The UPMH Fumane 2 deciduous lateral incisor postnatal crown formation time falls into the lower limit of the modern human range (28, 30). Overall, the enamel growth rates and the time to form postnatal enamel are comparable to modern human data, regardless of differences in their relative tissue volumes and morphologies (7–9).

Daily enamel secretion rates (DSRs) of all specimens, collected in the first 100-μm layer along the EDJ where laser tracks were run, are reported in Fig. 2*B*, compared with range of variation (min., mean, max.) of modern humans (27–30). Neanderthal DSRs in the first 100 μm of the enamel layer are slower than the corresponding modern human range of variability. However, when the entire dental crown is considered, the distributions of Neanderthal DSRs lie within the lower variability ranges of modern humans (Fig. 2*C*). The UPMH Fumane 2 DSRs fit the lower portion of the modern human ranges (Fig. 2 *B* and *C*). The postnatal crown formation times in Neanderthals couple with slower DSRs than in modern humans, as expected given the thinner enamel in Neanderthals' permanent and deciduous teeth (31, 32).

Weaning onset was determined using the topographical variation of the Sr/Ca ratio along the EDJ (15) (Fig. 3*A* and *SI*

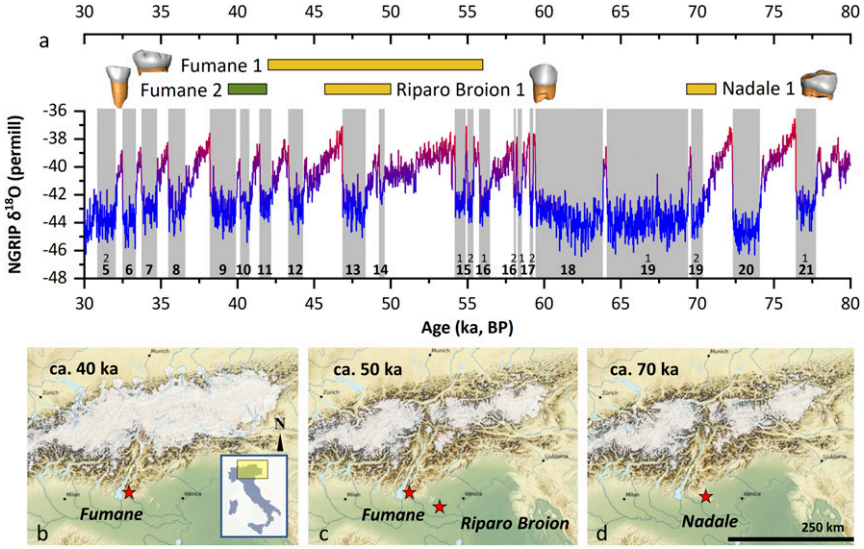

Fig. 1. Geographical, paleoecological, and chronological framework. (*A*) Oxygen isotope curve from North Greenland Ice Core Project (22), with Greenland Stadials 5 to 21 highlighted. Chronologies of the human specimens are also reported (as detailed in the *SI Appendix*); Fumane 2 is UPMH (green), while Nadale 1, Riparo Broion 1, and Fumane 1 are Neanderthals (yellow). (*B–D*) Modeled Alpine glacier extent during the time intervals of the teeth recovered at the sites of Fumane Cave (*B* and *C*), Riparo Broion (*C*), and Nadale (*D*); location within Italy is also shown (*Inset*). Simulations show a high temporal variability in the total modeled ice volume during Marine Isotope Stages 4 (70-ka snapshot) and 3 (50-40-ka snapshots) with glaciers flowing into the major valleys and possibly even onto the foreland (23).

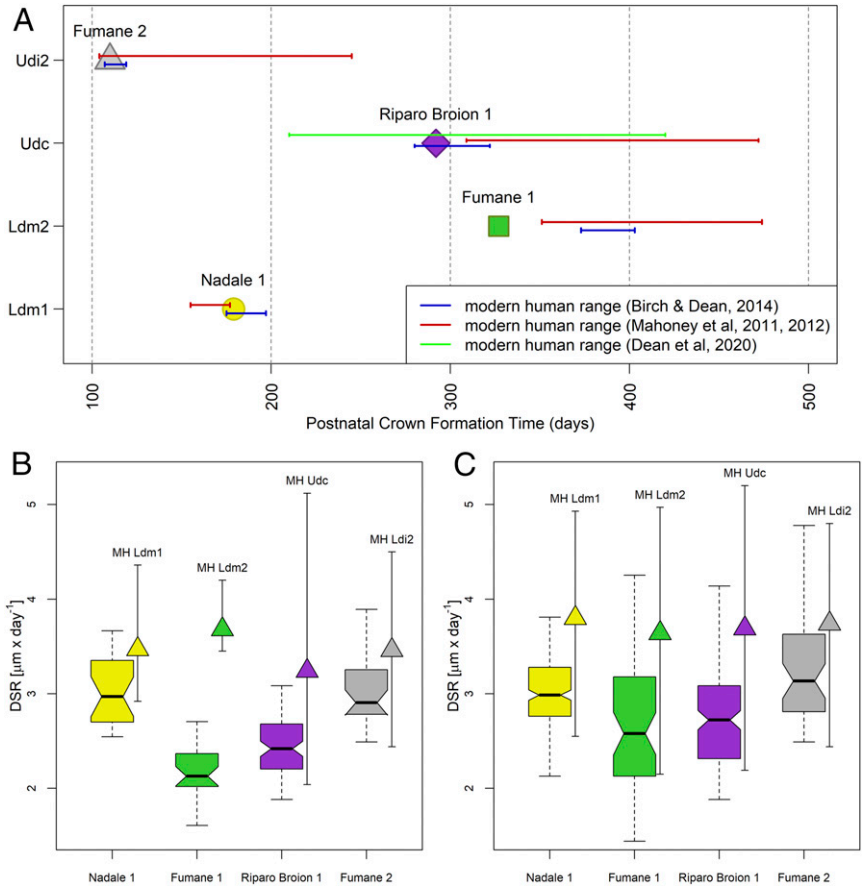

Fig. 2. Dental crown growth parameters. (*A*) Postnatal crown formation time in days from birth for the four investigated fossil deciduous teeth relative to the range of variability reported in literature for modern and archaeological individuals (red, blue, green lines). (*B*) Box plot of the daily secretion rate (DSR) variation in the first 100 µm from the enamel–dentine junction (min., second quartile, median, third quartile, max.) in comparison to the corresponding variability (min., mean, max.) of modern humans (MH), reassessed from refs. 27–30. (*C*) Box plot of the daily secretion rate variation across the whole crown (min., second quartile, median, third quartile, max.) and range of variation (min., mean, max.) of modern humans (MH), reassessed from refs. 27–30. Ldm1, lower deciduous first molar; Ldm2, lower deciduous second molar; Udc, upper deciduous canine; Ldi2, lower deciduous later incisor.

Appendix, Text S3). In exclusively breastfed newborns, the enamel Sr/Ca ratio is markedly lower relative to their prenatal levels (15, 33, 34). This is because human milk is highly enriched in Ca, i.e., Ca is selectively transferred, compared to Sr, across the mammary glands and the placenta (35, 36). Such behavior is confirmed by analyses of breastmilk and infant sera (37). In comparison to human milk, herbivore milk (and derived formula) is characterized by higher Sr/Ca levels due to the lower initial trophic position (38). Our dietary model for early life (Fig. 3*A* and *SI Appendix*, Text S3) agrees with the expected Sr behavior (15, 34, 39), showing a decrease in Sr/Ca during exclusive breastfeeding and changes in the slope of the profile across the major dietary transitions (i.e., introduction of solid food and end of weaning; additional discussion is provided in *SI Appendix*, Text S3) (34). This model has been tested successfully in this study on a set of contemporary children's teeth with known dietary histories, including their mothers' eating habits (*SI Appendix*, Text S3 and Figs. S6–S8). Alternative literature models for Ba/Ca point to an increase of Ba/Ca in postnatal enamel during breastfeeding (11, 12); yet, due to even stronger discrimination across biological membranes, Ba/Ca behavior is expected to be similar to Sr/Ca (34), as indeed unequivocally observed here (*SI Appendix*, Text S3 and Figs. S6–S8) and elsewhere (15, 40–42).

Nadale 1 (Fig. 3*B*), Fumane 1 (Fig. 3*C*), and Fumane 2 (Fig. 3*E*) are sufficiently well-preserved from a geochemical point of view. Riparo Broion 1 (Fig. 3*D*), in contrast, shows some diagenetic overprint, but the overall biogenic elemental pattern can still be discerned (Fig. 3*F*, where only the portions with [U] < 0.05 ppm are included in the interpolated profiles). Overall, Ba is more diagenetically affected than Sr (*SI Appendix*, Text S4, includes diagenesis assessment strategy and detailed description of the diagenetic overprints).

Two of the three Neanderthals, Fumane 1 and Riparo Broion 1, clearly show a decreasing trend in Sr/Ca ratio immediately postbirth, followed by slope changes with the first introduction of nonbreastmilk food at 115 d (3.8 mo) and 160 d (5.3 mo; Fig. 3 *C* and *D*), respectively. An even stronger signal of transitional food intake is visible in Fumane 1 at 200 d (6.6 mo) in the form of a steep increase in Sr/Ca ratio. For the oldest Neanderthal specimen, Nadale 1, following a marked variability before birth, the Sr/Ca profile slightly decreases until 140 d (4.7 mo; Fig. 3*B*). We cannot determine the weaning onset for this individual, who was still being exclusively breastfed by ~5 mo of life. The UPMH Fumane 2 has a substantial portion of the prenatal enamel preserved and only a short postnatal enamel growth record (~85 d vs. ~55 d respectively; Fig. 3*E*). This precludes the chemical detection of the onset of weaning, although the Sr/Ca drop at birth clearly indicates breastfeeding. The prenatal Sr/Ca increase in Fumane 2 could be related to changing dietary habits of the mother during pregnancy. A similar trend in prenatal enamel is observable in MCS2 (Fig. 3*A*), whose mother followed a diet poor in meat during pregnancy. The Sr isotope profiles of all investigated teeth

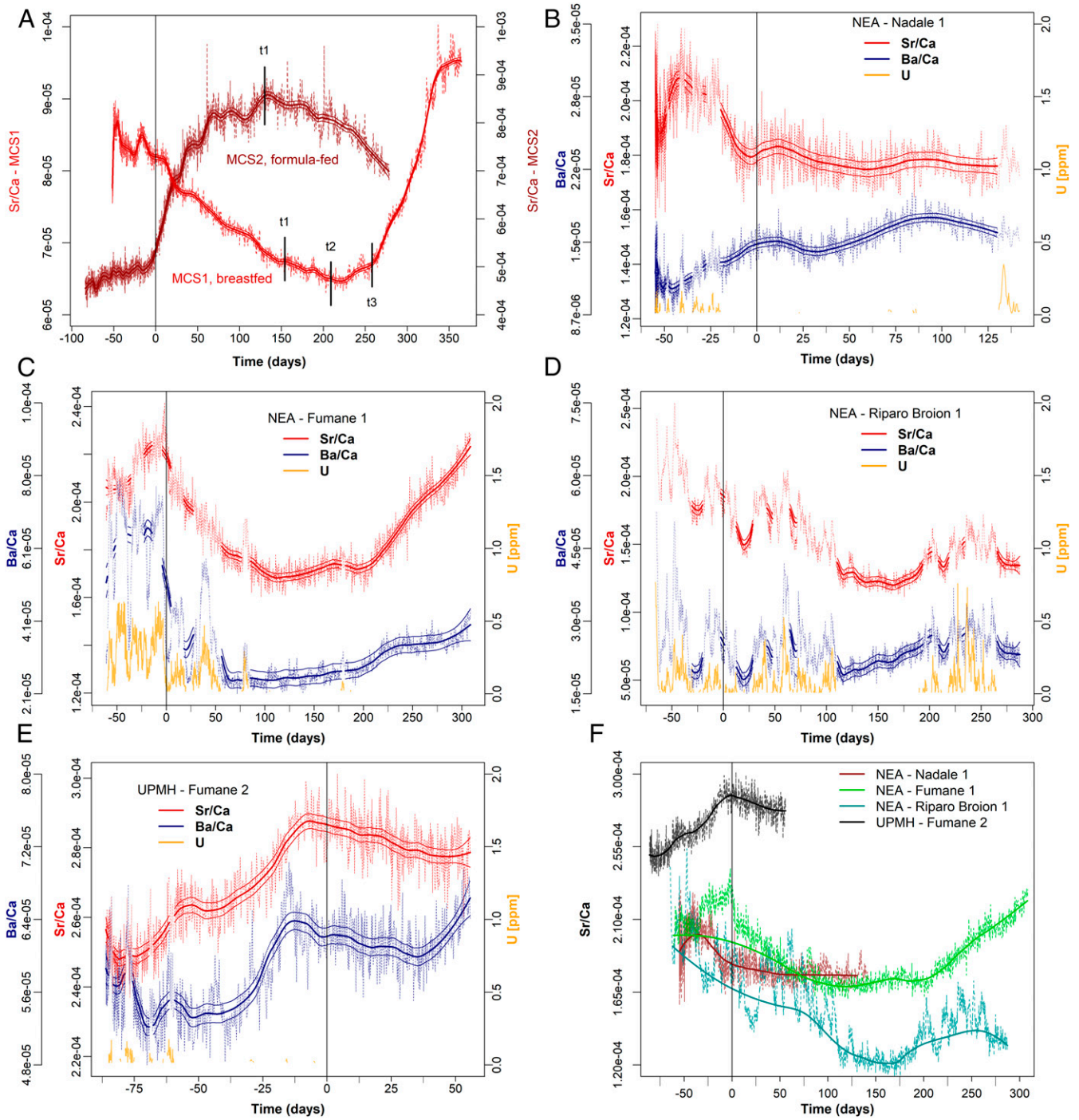

Fig. 3. Nursing histories from time-resolved Sr/Ca variation in Middle-Upper Paleolithic deciduous teeth. NEA, Neanderthal; UPMH, Upper Paleolithic modern human. The elemental profiles (Sr/Ca; Ba/Ca for comparison) were analyzed within enamel closest to the enamel–dentine junction (EDJ); [U] is reported as diagenetic alteration proxy for all fossil specimens (15) (*SI Appendix*, Text S4 and Fig. S13); diagenetically affected sections are grayed out. All are plotted relative to secretion time (in days); the birth event is highlighted by a vertical line in each plot. Elemental ratios are reported mass (weight)-based, not as mol/mol (15). The compositional profiles were smoothed with a locally weighted polynomial regression fit (LOWESS), with its associated SE range (±3 SE) for each predicted value. (*A*) Comparison between two contemporary individuals with known feeding histories, MCS1 (exclusively breastfed) and MCS2 (exclusively formula-fed); t1, transitional period, i.e., first time solid food starts; t2, progressively reduced breastfeeding during day; t3, transitional period ends, end of breastfeeding. (*B*) Nadale 1: the slight decrease of Sr/Ca indicates exclusive breastfeeding until the end of crown formation (4.7 mo). (*C*) Fumane 1: Sr/Ca variation indicates breastfeeding until 4 mo of age (fully comparable with MCS1 sample; *SI Appendix*, Fig. S6). (*D*) Riparo Broion 1: Sr/Ca profile indicates exclusive breastfeeding until 5 mo of age. (*E*) Fumane 2: 55 d of available postnatal enamel shows exclusive breastfeeding. (*F*) Comparative Sr/Ca profiles of all fossil specimens adjusted to the birth event; the interpolated modeled profiles were calculated based on those portions unaffected by diagenesis ([U] < 0.05 ppm), with strong smoothing parameters to reveal the biogenic signal. Riparo Broion 1, the specimen most affected by diagenesis, retains the overall outline of a breastfeeding signal (*A*). Further details are provided in *Materials and Methods*.

show very limited intrasample variability, confirming that Sr/Ca variations likely relate to changes in dietary end-members rather than diverse geographical provenance of food sources (Fig. 4). These data also give insights into Neanderthal mobility and resource gathering. The $^{87}Sr/^{86}Sr$ ratios of all Neanderthal teeth mostly overlap with the respective local baselines, defined through archaeological micromammals (43). This suggests that the mothers mostly exploited local food resources. Fumane 1 and Fumane 2, both from the same archaeological site, are characterized by different mean $^{87}Sr/^{86}Sr$ ratios (0.7093 vs. 0.7088), indicative of a different use of resources between Neanderthal (local resources) and early UPMH (nonlocal resources). Such behavior might have been driven by climatic fluctuations, suggesting colder conditions at ∼40 ka, dominated by steppe and Alpine meadows (44).

Discussion

Nursing strategies are strictly linked to fertility rates, maternal energetic investment, immune development, and infant mortality (45). All of these ultimately contribute to demographic changes of a specific population, with key relevance to the study of human evolution. Prolonged exclusive breastfeeding has a positive impact on an infant's immune system; however, longer breastfeeding negatively influences women's fertility via lactational amenorrhea and thus interbirth intervals (46). It has been shown that the age peak for weaning onset is reached at around 2.1 times birth weight (47), implying that infants who grow more rapidly need to be weaned earlier than those with a slower pace of growth. Based on modern models, a sustainable timing for infant weaning onset would thus range between 3 and 5 mo of age (4). However, contemporary nonindustrial societies start weaning their children at a modal age of 6 mo (6). Similarly, the World Health Organization recommends exclusive breastfeeding for the first 6 mo of an infant's life (48). This time frame broadly corresponds to the age at which the masticatory apparatus develops, favoring the chewing of first solid foods (4). Such evidence suggests that both skeletal development and infant energy demand contribute to the beginning of the weaning transition. Introduction of nonbreastmilk foods is also crucial in reducing the energetic burden of lactation for the mother (6). Breastfeeding represents a substantial investment of energy resources (total caloric content of modern human breastmilk, ∼60 kcal/100 mL) (49), entailing an optimal energy allocation between baby feeding and other subsistence-related activities.

Our time-resolved chemical data point to an introduction of nonbreastmilk foods at ∼5 to 6 mo in the infant diet of two Neanderthals, sooner than previously observed (11, 12) and fully within the modern human preindustrial figures (6). Neanderthals, therefore, were capable of being weaned at least from the fifth postnatal month in terms of supplementing the nutritional requirements of an infant that is growing a large brain with high energy requirements. This evidence, combined with deciduous dental growth akin to modern humans, indicates similar metabolic constraints for the two taxa during early life. The differential food exploitation of Fumane 1 and Fumane 2 mothers suggests a different human–environment interaction between Neanderthals and early UPMHs, as seen in Sr isotope profiles. The UPMH Fumane 2 mother was consuming low-biopurified nonlocal foodstuff with elevated Sr/Ca and possibly spent the end of her pregnancy and the first 23 d after delivery away from the Fumane site. The most parsimonious interpretation is that mother and child of Fumane 2 likely lived away from Fumane Cave and that, many years after, the UPMH child lost his tooth at Fumane Cave, away from his original birthplace. Conversely, all Neanderthal mothers spent the last part of their pregnancies and the lactation periods locally and were consuming high-biopurified local food (see low Sr/Ca-values in Fig. 3*F*). Such evidence of a seeming limited mobility for these Neanderthal women counters previous hypotheses of a large home-range of Neanderthals (50, 51).

The introduction of nonbreastmilk food at ∼5 to 6 mo implies relatively short interbirth intervals for Neanderthals due to an

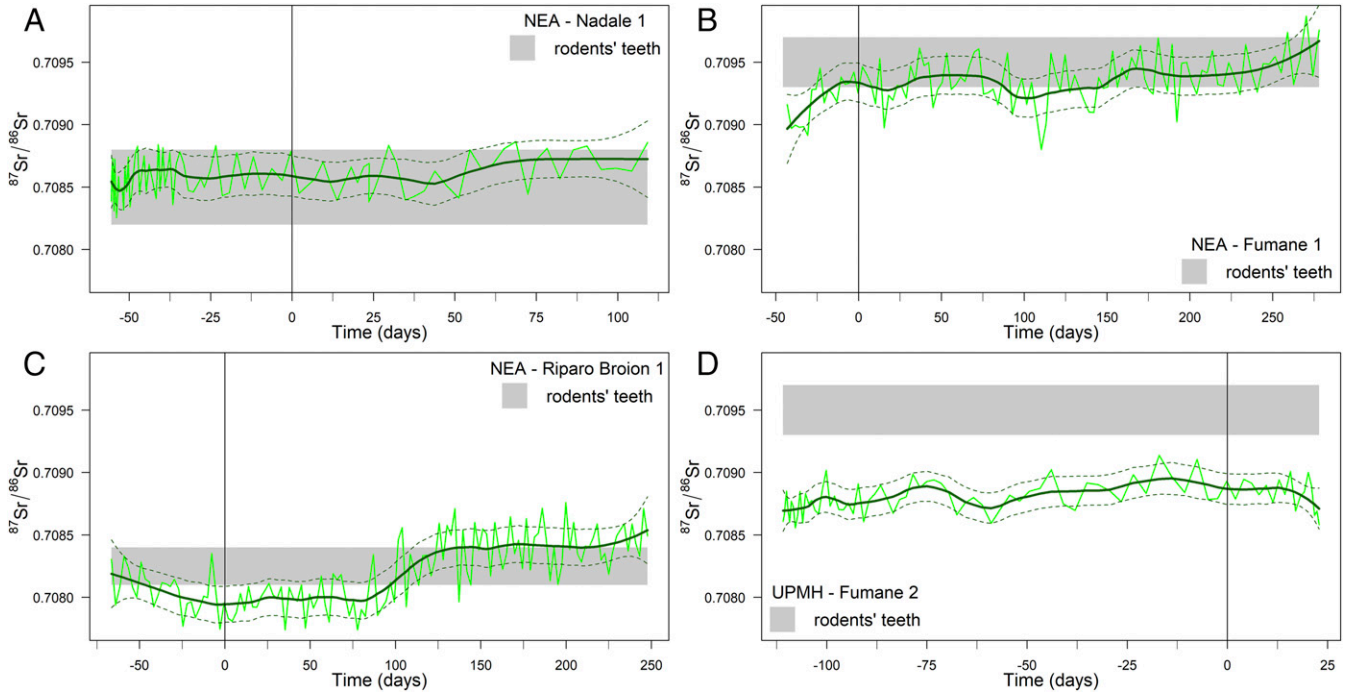

Fig. 4. Mobility of the Middle-Upper Paleolithic infants via time-resolved $^{87}Sr/^{86}Sr$ profiles of their deciduous teeth. Gray horizontal bands represent the local Sr isotopic baselines defined via the Sr isotopic composition of archaeological rodent enamel (*SI Appendix*, Table S1). The birth event is indicated by a vertical line. (*A* and *B*) Nadale 1/Fumane 1: exploitation of local food resources through the entire period; (*C*) Riparo Broion 1: possible limited seasonal mobility (nonlocal values between ca. −45 and 85 d, ∼4 mo); (*D*) Fumane 2: exploitation of nonlocal food resources through the entire period.

earlier resumption of postpartum ovulation (52). Moreover, considering the birth weight model (47), we hypothesize that Neanderthal newborns were of similar weight to modern human neonates, pointing to a likely similar gestational history and early-life ontogeny. In a broader context, our results suggest that nursing mode and time among Late Pleistocene humans in Europe were likely not influenced by taxonomic differences in physiology. Therefore, our findings do not support the hypothesis that long postpartum infertility was a contributing factor to the demise of Neanderthals (13). On the contrary, genetic evidence indicates that Neanderthal groups were limited in size (53), which is not in agreement with the shorter interbirth interval proposed here. Thus, other factors such as cultural behavior, shorter lifespan, and high juvenile mortality might have played a focal role in limiting Neanderthal's group size (54, 55).

Materials and Methods

Thin Slices of Teeth Preparation. Prior to sectioning, a photographic record of the samples was collected. Thin sections of the dental crowns were obtained using the standard method in dental histology described previously (56, 57) and prepared at the Service of Bioarchaeology of the Museo delle Civiltà in Rome. The sectioning protocol consists of a detailed embedding-cutting-mounting procedure that makes use of dental adhesives, composite resins, and embedding resins. In order to be able to remove the crown from the resin block after sectioning and to restore the dental crowns, the teeth were initially embedded with a reversible resin (Crystalbond 509; SPI Supplies) that does not contaminate chemically the dental tissues and is soluble in Crystalbond cleaning agent (Aramco Products). A second embedding in epoxy resin (EpoThin 2; Buehler) guarantees the stability of the sample during the cutting procedure. The sample was cured for 24 h at room temperature. Teeth were sectioned using an IsoMet low-speed diamond blade microtome (Buehler). After the first cut, a microscope slide previously treated with liquid silane (RelyX Ceramic Primer; 3M) was attached on the exposed surface using a light curing adhesive (Scotchbond Multi-Purpose Adhesive; 3M) to prevent cracks and any damage during the cutting procedure. A single longitudinal buccolingual thin section, averaging 250 μm thick, was cut from each specimen. Each ground section was reduced to a thickness of ∼150 μm using water-resistant abrasive paper of different grits (Carbimet; Buehler). Finally, the sections were polished with a microtissue (Buehler) and diamond paste with 1-μm size (DB-Suspension, M; Struers).

Each thin section was digitally recorded through a camera (Nikon DSFI3) paired with a transmitted light microscope (Olympus BX 60) under polarized light, with different magnifications (40×, 100×, and 400×, including the ocular magnifications). Overlapping pictures of the dental crown were assembled in a single micrograph using the software ICE 2.0 (Image Composite Editor; Microsoft Research Computational Photography Group; *SI Appendix*, Fig. S1).

After sectioning, the crowns were released from the epoxy block using the Crystalbond cleaning agent and reconstructed using light-curing dental restoration resin (Heraeus Charisma Dental Composite Materials).

Concerning modern teeth, formal consent was given by all relevant people with legal authority who gave their explicit written consent. All individual data were treated in a fully anonymous way and it is not possible from the present results to identify the individuals concerned.

Sr Isotopic Analysis by Solution MC-ICPMS. To determine local Sr isotope baselines, we analyzed archaeological rodent teeth from the same sites where the human teeth were found (*SI Appendix*, Table S1). Samples were prepared at the Department of Chemical and Geological Sciences of the University of Modena and Reggio Emilia following protocols described elsewhere (16, 58) and briefly summarized here.

From each archaeological site, we selected several rodent teeth according to the stratigraphic distribution of human samples. Enamel from micromammal incisors was manually removed using a scalpel. Few teeth were also analyzed as whole (dentine + enamel). Before the actual dissolution with 3 M HNO_3, samples (1 to 5 mg in mass) were washed with MilliQ (ultrasonic bath) and leached with ∼0.5 M HNO_3. Sr of the dissolved specimens was separated from the matrix using 30-μL columns and Eichrom Sr-Spec resin.

Sr isotope ratios were measured using a Neptune multicollector inductively coupled plasma mass spectrometer (MC-ICPMS; ThermoFisher) housed at the Centro Interdipartimentale Grandi Strumenti (UNIMORE) during different analytical sessions. Seven Faraday detectors were used to collect signals of the following masses: ^{82}Kr, ^{83}Kr, ^{84}Sr, ^{85}Rb, ^{86}Sr, ^{87}Sr, and ^{88}Sr. Sr solutions were diluted to ∼50 ppb and introduced into the Neptune through an APEX desolvating system. Corrections for Kr and Rb interferences follow previous works (16). Mass bias corrections used an exponential law and a $^{88}Sr/^{86}Sr$ ratio of 8.375209 (59). The Sr ratios of samples were reported to a SRM987 value of 0.710248 (60). During one session, SRM987 yielded an average $^{87}Sr/^{86}Sr$ ratio of 0.710243 ± 0.000018 (2 SD; n = 8). Total laboratory Sr blanks did not exceed 100 pg.

Spatially Resolved Sr Isotopic Analysis by Laser-Ablation Plasma Mass Spectrometry (LA-MC-ICPMS). LA-MC-ICPMS analyses were conducted at the Frankfurt Isotope and Element Research Center (FIERCE) at Goethe University, Frankfurt am Main (Germany), and closely follow analytical protocols described by Müller and Anczkiewicz (17); only a brief summary is provided here, aiming at highlighting project-specific differences. A 193-nm ArF excimer laser (RESOlution S-155; formerly Resonetics, ASI, now Applied Spectra) equipped with a two-volume LA cell (Laurin Technic) was connected to a NeptunePlus MC-ICPMS (ThermoFisher) using Nylon 6 tubing and a "squid" signal-smoothing device (61). Ablation took place in a He atmosphere (300 mL/min), with ∼1,000 mL/min Ar added at the funnel of the two-volume LA cell and 3.5 mL/min N_2 before the squid. Laser fluence on target was ∼5 J/cm^2.

Spatially resolved Sr isotopic analyses of dental enamel were performed on the thin sections (100 to 150 μm thick) used for enamel histology and trace element analysis (see below) in continuous profiling mode following the enamel–dentine junction (EDJ) from apex to cervix (14), less than 100 μm away from the EDJ. Tuning of the LA-MC-ICPMS used NIST 616 glass for best sensitivity (^{88}Sr) while maintaining robust plasma conditions, i.e., $^{232}Th^{16}O/^{232}Th$ <0.5% and $^{232}Th/^{238}U$ >0.95 with RF power of ∼1,360 W. In view of the low Sr concentrations in these human enamel samples (∼60 to 100 μg/g), we utilized 130-μm spots, a scan speed of 5 μm/s, and a repetition rate of 20 Hz to maintain ^{88}Sr ion currents of ∼2 to 3.5 × 10^{-11} A. Nine Faraday detectors were used to collect the ion currents of the following masses (m/z): ^{83}Kr, ∼83.5, ^{84}Sr, ^{85}Rb, ^{86}Sr, ∼86.5, ^{87}Sr, ^{88}Sr, ^{90}Zr. Baseline, interference, and mass bias corrections follow ref. 17. The isotopically homogenous (Sr) enameloid of a modern shark was used to assess accuracy of the Sr isotopic analysis and yielded $^{87}Sr/^{86}Sr = 0.70916 \pm 2$ and $^{84}Sr/^{86}Sr = 0.0565 \pm 1$ (2 SD). Raw data are reported in Dataset S1.

Spatially Resolved Elemental Ratio and Concentration Analysis by Laser-Ablation Plasma Mass Spectrometry (LA- ICPMS). All LA-ICPMS analyses of archaeological samples were conducted at the Frankfurt Isotope and Element Research Center (FIERCE) at Goethe University, Frankfurt am Main (Germany), using the same LA system described above, but connected via a squid smoothing device to an Element XR ICPMS. Analytical protocols follow those by Müller et al. (15), and only a brief summary is provided here aimed at highlighting differences. LA-ICPMS trace element ratios/concentrations of the comparative contemporary teeth were obtained at Royal Holloway University of London (RHUL) using the RESOlution M-50 prototype LA system featuring a Laurin two-volume LA cell (61) coupled to an Agilent 8900 triple-quadrupole ICPMS (ICP-QQQ or ICP-MS/MS).

Compositional profiles were analyzed parallel and as close as possible to the EDJ, following the same tracks used for Sr isotope analyses. We employed 15-μm spot sizes (FIERCE) or 6-μm (MCS3, RHUL) and 34-μm (MCS1 and 2, RHUL), respectively, as well as a scan speed of 5 μm/s and a repetition rate of 15 Hz; prior to acquisition, samples were precleaned using slightly larger spot sizes (22 to 57 μm), 20 Hz, and faster scan speeds (25 to 50 μm/s); laser fluence was ∼5 J/cm^2. The following isotopes (m/z) were analyzed: ^{25}Mg, ^{27}Al, ^{43}Ca, (^{44}Ca), ^{55}Mn, ^{66}Zn, ^{85}Rb, (^{86}Sr), ^{88}Sr, ^{89}Y, ^{138}Ba, ^{140}Ce, (^{166}Er, ^{172}Yb), ^{208}Pb, and ^{238}U. The total sweep times for the Element XR and the 8900 ICP-MS/MS were ∼0.8 and 0.4 to 0.5 s, respectively; however, because of the slow scan speeds, this small difference has no effect on the compositional profiles presented here. Primary standardization was achieved using NIST SRM612. Ca was employed as internal standard (^{43}Ca); [Ca] at 37% m/m was used to calculate concentrations for unknown bioapatites, although not required for X/Ca ratios. Accuracy and reproducibility were assessed using repeated analyses of the STDP-X-glasses (62) as secondary reference materials; the respective values for Sr/Ca and Ba/Ca (the element/Ca ratios of principal interest) here are 1.8 ± 6.6% and −0.2 ± 6.0% [%bias ± 2 SD (%)]; this compares well with the long-term reproducibility for these analytes reported previously (63). Raw data are reported in Datasets S2 and S3.

The compositional/isotopic profiles were smoothed with a locally weighted polynomial regression fit (LOWESS) with its associated SE range (±3 SE) for each predicted value (64). The statistical package R (ver. 44.0.0) (65) was used for all statistical computations and generation of graphs.

Assessment of the Enamel Growth Parameters and of the Chronologies along the Laser Tracks. Dental enamel is capable of recording, at microscopic level during its formation, regular physiological and rhythmic growth markers

(66–68). These incremental markings are visible under transmitted light in longitudinal histological thin sections of dental crowns. Enamel forms in a rhythmic manner, reflecting the regular incremental secretion of the matrix by the ameloblasts (i.e., the enamel-forming cells). The rhythmical growth of enamel is expressed in humans at two different levels: a circadian rhythm that produces the daily cross-striations (69, 70) and a longer period rhythmic marking (near-weekly in humans) that give rise to the Retzius lines (71). Physiological stresses affecting the individual during tooth growth cause a disruption of the enamel matrix secretion and mark the corresponding position of the secretory ameloblast front, producing accentuated (Retzius) lines (ALs) (72, 73). The birth event is recorded in the forming enamel of individuals surviving the perinatal stage, and leaves an accentuated line (usually the first), namely the neonatal line (NL) (26, 74, 75).

The time taken to form the dental crown after birth was measured on each thin section, adapting the methods described in the literature (30, 76).

A prism segment starting from the most apical available point on the enamel–dentine junction (EDJ) and extending from this point to an isochronous incremental line (i.e., the NL, an AL or a Retzius line) was measured. The incremental line was followed back to the EDJ, and a second prism segment was measured in the same way. The process was repeated until the most cervical enamel was reached. The crown formation time is equal to the sum of the single prism segments. To obtain time (in days) from the prism length measurements, local daily secretion rates (25) (DSRs) were calculated around the prism segments and within 100 μm from the EDJ by counting visible consecutive cross-striations and dividing the count by the corresponding prism length. The chronologies of accentuated lines (ALs) in the modern sample closely match the timing of known disruptive life history events in the mother (illness, surgery) and infant, and so are well within the range or error (1.2 to 4.4%) observed for this histological aging method (67).

DSRs were collected across the whole crown on spots chosen randomly in order to get the DSR distribution. Groups of cross-striations ranging from 3 to 7 were measured. For each crown, the number of measured spots ranges between 49 and 233.

After LA-ICPMS analyses, a micrograph highlighting the laser tracks was acquired at 50× magnification. This was superimposed to a second micrograph of the same thin section at 100× magnification to gain better visibility of the enamel microstructural features. The chronologies along the laser tracks were obtained matching the tracks with the isochronous lines.

Data Availability. All study data are included in the article and supporting information.

ACKNOWLEDGMENTS. Archaeological excavations at Fumane and De Nadale are coordinated by the University of Ferrara and supported by public institutions (Fumane, Lessinia Mountain Community, Fumane Municipality, BIMAdige; De Nadale, Zovencedo Municipality) and private associations and companies (De Nadale, 'Realizzazioni Artigiane Articoli Speciali Meccanici'). Archaeological excavations at Riparo Broion are coordinated by the University of Bologna and University of Ferrara and supported by H2020 Grant 724046–SUCCESS. 'Soprintendenza Archeologia, Belle Arti e Paesaggio per le province di Verona, Rovigo e Vicenza' provided access to the samples of Nadale 1, Riparo Broion 1, Fumane 1, and Fumane 2. We thank the parents and the children who donated deciduous teeth and carefully recorded the dietary events of their children. Michael P. Richards and Marcello Mannino are thanked for stimulating discussions and for having initiated isotopic studies of the specimens at Fumane. This project was funded by the European Research Council (ERC) under the European Union's Horizon 2020 Research and Innovation Programme (Grant Agreement no. 724046–SUCCESS awarded to S.B.; wwwerc-success.eu and Grant Agreement no. 639286–HIDDEN FOODS awarded to E.C.; www.hiddenfoods.org). The Frankfurt Isotope & Element Research Center is financially supported by the the Wilhelm and Else Heraeus Foundation and by the Deutsche Forschungsgemeinschaft (DFG; INST 161/921-1 Forschungsgroßgeräte and INST 161/923-1 Forschungsgroßgeräte), which is gratefully acknowledged. Laser ablation-inductively coupled plasma mass spectrometry analyses at Royal Holloway University of London, used for comparative modern samples, were supported by theNatural Environment Research Council (NERC) equipment funding (NERC CC073). The Marie Skłodowska-Curie Actions–European Commission provided a research grant to A.N. (Grant H2020-MSCA-IF-2018-842812). The Radiogenic Isotope Laboratory of the University of Modena and Reggio Emilia has been funded through a grant of the "Programma Giovani Ricercatori Rita Levi Montalcini" (to A.C.).

1. D. W. Sellen, Evolution of infant and young child feeding: Implications for contemporary public health. *Annu. Rev. Nutr.* **27**, 123–148 (2007).
2. G. E. Kennedy, From the ape's dilemma to the weanling's dilemma: Early weaning and its evolutionary context. *J. Hum. Evol.* **48**, 123–145 (2005).
3. C. W. Kuzawa *et al.*, Metabolic costs and evolutionary implications of human brain development. *Proc. Natl. Acad. Sci. U.S.A.* **111**, 13010–13015 (2014).
4. L. T. Humphrey, Weaning behaviour in human evolution. *Semin. Cell Dev. Biol.* **21**, 453–461 (2010).
5. D. P. Davies, B. O'Hare, Weaning: A worry as old as time. *Curr. Paediatr.* **14**, 83–96 (2004).
6. D. W. Sellen, Comparison of infant feeding patterns reported for nonindustrial populations with current recommendations. *J. Nutr.* **131**, 2707–2715 (2001).
7. T. M. Smith *et al.*, Dental evidence for ontogenetic differences between modern humans and Neanderthals. *Proc. Natl. Acad. Sci. U.S.A.* **107**, 20923–20928 (2010).
8. R. Macchiarelli *et al.*, How Neanderthal molar teeth grew. *Nature* **444**, 748–751 (2006).
9. A. Rosas *et al.*, The growth pattern of Neandertals, reconstructed from a juvenile skeleton from El Sidrón (Spain). *Science* **357**, 1282–1287 (2017).
10. M. S. Ponce de León, T. Bienvenu, T. Akazawa, C. P. Zollikofer, Brain development is similar in Neanderthals and modern humans. *Curr. Biol.* **26**, R665–R666 (2016).
11. T. M. Smith *et al.*, Wintertime stress, nursing, and lead exposure in Neanderthal children. *Sci. Adv.* **4**, eaau9483 (2018).
12. C. Austin *et al.*, Barium distributions in teeth reveal early-life dietary transitions in primates. *Nature* **498**, 216–219 (2013).
13. M. Skinner, Dental wear in immature Late Pleistocene European hominines. *J. Archaeol. Sci.* **24**, 677–700 (1997).
14. M. C. Dean, Retrieving chronological age from dental remains of early fossil hominins to reconstruct human growth in the past. *Philos. Trans. R. Soc. Lond. B Biol. Sci.* **365**, 3397–3410 (2010).
15. W. Müller *et al.*, Enamel mineralization and compositional time-resolution in human teeth evaluated via histologically-defined LA-ICPMS profiles. *Geochim. Cosmochim. Acta* **255**, 105–126 (2019).
16. F. Lugli *et al.*, Strontium and stable isotope evidence of human mobility strategies across the Last Glacial Maximum in southern Italy. *Nat. Ecol. Evol.* **3**, 905–911 (2019).
17. W. Müller, R. Anczkiewicz, Accuracy of laser-ablation (LA)-MC-ICPMS Sr isotope analysis of (bio) apatite–a problem reassessed. *J. Anal. At. Spectrom.* **31**, 259–269 (2016).
18. J. Arnaud *et al.*, A Neanderthal deciduous human molar with incipient carious infection from the Middle Palaeolithic De Nadale cave, Italy. *Am. J. Phys. Anthropol.* **162**, 370–376 (2017).
19. S. Benazzi *et al.*, Middle Paleolithic and Uluzzian human remains from Fumane Cave, Italy. *J. Hum. Evol.* **70**, 61–68 (2014).
20. M. Romandini *et al.*, A late Neanderthal tooth from northeastern Italy. *J. Hum. Evol.* **147**, 102867 (2020).
21. S. Benazzi *et al.*, Archaeology. The makers of the Protoaurignacian and implications for Neandertal extinction. *Science* **348**, 793–796 (2015).
22. S. O. Rasmussen *et al.*, A stratigraphic framework for abrupt climatic changes during the Last Glacial period based on three synchronized Greenland ice-core records: Refining and extending the INTIMATE event stratigraphy. *Quat. Sci. Rev.* **106**, 14–28 (2014).
23. J. Seguinot *et al.*, Modelling last glacial cycle ice dynamics in the Alps. *Cryosphere* **12**, 3265–3285 (2018).
24. J. W. Wood *et al.*, The Osteological Paradox: Problems of inferring prehistoric health from skeletal samples [and Comments and Reply]. *Curr. Anthropol.* **33**, 343–370 (1992).
25. A. Nava *et al.*, New regression formula to estimate the prenatal crown formation time of human deciduous central incisors derived from a Roman Imperial sample (Velia, Salerno, Italy, I-II cent. CE). *PLoS One* **12**, e0180104 (2017).
26. M. C. Dean, K. M. Spiers, J. Garrevoet, A. Le Cabec, Synchrotron X-ray fluorescence mapping of Ca, Sr and Zn at the neonatal line in human deciduous teeth reflects changing perinatal physiology. *Arch. Oral Biol.* **104**, 90–102 (2019).
27. P. Mahoney, Human deciduous mandibular molar incremental enamel development. *Am. J. Phys. Anthropol.* **144**, 204–214 (2011).
28. P. Mahoney, Incremental enamel development in modern human deciduous anterior teeth. *Am. J. Phys. Anthropol.* **147**, 637–651 (2012).
29. M. C. Dean, L. Humphrey, A. Groom, B. Hassett, Variation in the timing of enamel formation in modern human deciduous canines. *Arch. Oral Biol.* **114**, 104719 (2020).
30. W. Birch, M. C. Dean, A method of calculating human deciduous crown formation times and of estimating the chronological ages of stressful events occurring during deciduous enamel formation. *J. Forensic Leg. Med.* **22**, 127–144 (2014).
31. C. Fornai *et al.*, Enamel thickness variation of deciduous first and second upper molars in modern humans and Neanderthals. *J. Hum. Evol.* **76**, 83–91 (2014).
32. A. J. Olejniczak *et al.*, Dental tissue proportions and enamel thickness in Neandertal and modern human molars. *J. Hum. Evol.* **55**, 12–23 (2008).
33. L. T. Humphrey, M. C. Dean, T. E. Jeffries, M. Penn, Unlocking evidence of early diet from tooth enamel. *Proc. Natl. Acad. Sci. U.S.A.* **105**, 6834–6839 (2008).
34. L. T. Humphrey, Isotopic and trace element evidence of dietary transitions in early life. *Ann. Hum. Biol.* **41**, 348–357 (2014).
35. E. Rossipal, M. Krachler, F. Li, D. Micetic-Turk, Investigation of the transport of trace elements across barriers in humans: Studies of placental and mammary transfer. *Acta Paediatr.* **89**, 1190–1195 (2000).
36. L. T. Humphrey, W. Dirks, M. C. Dean, T. E. Jeffries, Tracking dietary transitions in weanling baboons (Papio hamadryas anubis) using strontium/calcium ratios in enamel. *Folia Primatol. (Basel)* **79**, 197–212 (2008).

37. M. Krachler, E. Rossipal, D. Micetic-Turk, Concentrations of trace elements in sera of newborns, young infants, and adults. *Biol. Trace Elem. Res.* **68**, 121–135 (1999).
38. J. H. Burton, T. D. Price, W. D. Middleton, Correlation of bone Ba/Ca and Sr/Ca due to biological purification of calcium. *J. Archaeol. Sci.* **26**, 609–616 (1999).
39. T. Tsutaya, M. Yoneda, Reconstruction of breastfeeding and weaning practices using stable isotope and trace element analyses: A review. *Am. J. Phys. Anthropol.* **156** (suppl. 59), 2–21 (2015).
40. S. Peek, M. T. Clementz, Sr/Ca and Ba/Ca variations in environmental and biological sources: A survey of marine and terrestrial systems. *Geochim. Cosmochim. Acta* **95**, 36–52 (2012).
41. J. Z. Metcalfe, F. J. Longstaffe, G. D. Zazula, Nursing, weaning, and tooth development in woolly mammoths from Old Crow, Yukon, Canada: Implications for Pleistocene extinctions. *Palaeogeogr. Palaeoclimatol. Palaeoecol.* **298**, 257–270 (2010).
42. T. Tacail, L. Kovačiková, J. Brůžek, V. Balter, Spatial distribution of trace element Ca-normalized ratios in primary and permanent human tooth enamel. *Sci. Total Environ.* **603-604**, 308–318 (2017).
43. J. M. López-García, C. Berto, M. Peresani, Environmental and climatic context of the hominin occurrence in northeastern Italy from the late Middle to Late Pleistocene inferred from small-mammal assemblages. *Quat. Sci. Rev.* **216**, 18–33 (2019).
44. J. M. López-García, C. dalla Valle, M. Cremaschi, M. Peresani, Reconstruction of the Neanderthal and Modern Human landscape and climate from the Fumane cave sequence (Verona, Italy) using small-mammal assemblages. *Quat. Sci. Rev.* **128**, 1–13 (2015).
45. E. M. Miller, *Beyond Passive Immunity: Breastfeeding, Milk and Collaborative Mother-Infant Immune Systems. Breastfeeding: New Anthropological Approaches*, (Routledge, New York, 2018), pp. 26–39.
46. K. L. Campbell, J. W. Wood, *Fertility in Traditional Societies. Natural Human Fertility*, (Springer, 1988), pp. 39–69.
47. P. C. Lee, The meanings of weaning: Growth, lactation, and life history. *Evol. Anthropol. News Rev. (Melb.)* **5**, 87–98 (1996).
48. World Health Organization, Infant and young child feeding: Model chapter for textbooks for medical students and allied health professionals (WHO, Geneva, 2009).
49. P. Prentice *et al*., Breast milk nutrient content and infancy growth. *Acta Paediatr.* **105**, 641–647 (2016).
50. M. Richards *et al*., Strontium isotope evidence of Neanderthal mobility at the site of Lakonis, Greece using laser-ablation PIMMS. *J. Archaeol. Sci.* **35**, 1251–1256 (2008).
51. C. Wißing *et al*., Stable isotopes reveal patterns of diet and mobility in the last Neandertals and first modern humans in Europe. *Sci. Rep.* **9**, 4433 (2019).
52. H. W. Taylor, M. Vázquez-Geffroy, S. J. Samuels, D. M. Taylor, Continuously recorded suckling behaviour and its effect on lactational amenorrhoea. *J. Biosoc. Sci.* **31**, 289–310 (1999).
53. K. Prüfer *et al*., The complete genome sequence of a Neanderthal from the Altai Mountains. *Nature* **505**, 43–49 (2014).
54. C. M. Garber, Eskimo infanticide. *Sci. Mon.* **64**, 98–102 (1947).
55. E. Trinkaus, Neanderthal mortality patterns. *J. Archaeol. Sci.* **22**, 121–142 (1995).
56. A. Nava, "Hominin dental enamel: an integrated approach to the study of formation, maturation, and morphology (Unpublished doctoral dissertation)," PhD dissertation, Sapienza University of Rome, Rome (2018).
57. S. Caropreso *et al*., Thin sections for hard tissue histology: A new procedure. *J. Microsc.* **199**, 244–247 (2000).
58. M. Weber, F. Lugli, K. P. Jochum, A. Cipriani, D. Scholz, Calcium carbonate and phosphate reference materials for monitoring bulk and microanalytical determination of Sr isotopes. *Geostand. Geoanal. Res.* **42**, 77–89 (2018).
59. R. H. Steiger, E. Jäger, Subcommission on geochronology: Convention on the use of decay constants in geo-and cosmochronology. *Earth Planet. Sci. Lett.* **36**, 359–362 (1977).
60. J. M. McArthur, R. Howarth, T. Bailey, Strontium isotope stratigraphy: LOWESS version 3: Best fit to the marine Sr-isotope curve for 0–509 Ma and accompanying look-up table for deriving numerical age. *J. Geol.* **109**, 155–170 (2001).
61. W. Müller, M. Shelley, P. Miller, S. Broude, Initial performance metrics of a new custom-designed ArF excimer LA-ICPMS system coupled to a two-volume laser-ablation cell. *J. Anal. At. Spectrom.* **24**, 209–214 (2009).
62. S. Klemme *et al*., Synthesis and preliminary characterisation of new silicate, phosphate and titanite reference glasses. *Geostand. Geoanal. Res.* **32**, 39–54 (2008).
63. D. Evans, W. Müller, Automated extraction of a five-year LA-ICP-MS trace element data set of ten common glass and carbonate reference materials: Long-term data quality, optimisation and laser cell homogeneity. *Geostand. Geoanal. Res.* **42**, 159–188 (2018).
64. W. S. Cleveland, E. Grosse, W. M. Shyu, Local regression models. *Statistical Models in S* **2**, 309–376 (1992).
65. R-Core-Team, *R: A Language and Environment for Statistical Computing*, (R Foundation for Statistical Computing, Vienna, Austria, 2020).
66. D. Antoine, S. Hillson, M. C. Dean, The developmental clock of dental enamel: A test for the periodicity of prism cross-striations in modern humans and an evaluation of the most likely sources of error in histological studies of this kind. *J. Anat.* **214**, 45–55 (2009).
67. M. Christopher Dean, Tooth microstructure tracks the pace of human life-history evolution. *Proc. Biol. Sci.* **273**, 2799–2808 (2006).
68. S. Hillson, *Tooth Development in Human Evolution and Bioarchaeology*, (Cambridge University Press, Cambridge, 2014).
69. R. S. Lacruz *et al*., The circadian clock modulates enamel development. *J. Biol. Rhythms* **27**, 237–245 (2012).
70. L. Zheng *et al*., Circadian rhythms regulate amelogenesis. *Bone* **55**, 158–165 (2013).
71. M. C. Dean, Growth layers and incremental markings in hard tissues; a review of the literature and some preliminary observations about enamel structure in *Paranthropus boisei*. *J. Hum. Evol.* **16**, 157–172 (1987).
72. A. Nava, D. W. Frayer, L. Bondioli, Longitudinal analysis of the microscopic dental enamel defects of children in the Imperial Roman community of Portus Romae (necropolis of Isola Sacra, 2nd to 4th century CE, Italy). *J. Archaeol. Sci. Rep.* **23**, 406–415 (2019).
73. C. Witzel *et al*., Reconstructing impairment of secretory ameloblast function in porcine teeth by analysis of morphological alterations in dental enamel. *J. Anat.* **209**, 93–110 (2006).
74. N. Sabel *et al*., Neonatal lines in the enamel of primary teeth–a morphological and scanning electron microscopic investigation. *Arch. Oral Biol.* **53**, 954–963 (2008).
75. C. Zanolli, L. Bondioli, F. Manni, P. Rossi, R. Macchiarelli, Gestation length, mode of delivery, and neonatal line-thickness variation. *Hum. Biol.* **83**, 695–713 (2011).
76. D. Guatelli-Steinberg, B. A. Floyd, M. C. Dean, D. J. Reid, Enamel extension rate patterns in modern human teeth: Two approaches designed to establish an integrated comparative context for fossil primates. *J. Hum. Evol.* **63**, 475–486 (2012).